Modelling and minimization of the parasitic capacitance of ring core inductors

Florentin Salomez, Arnaud Videt, Nadir Idir

Modelling and minimization of the parasitic capacitance of ring core inductors

Florentin SALOMEZ, Arnaud VIDET, Nadir IDIR
Univ. Lille, Arts et Metiers Institute of Technology, Centrale Lille, Junia, ULR 2697 - L2EP
Lille, France
Email: florentin.salomez@univ-lille.fr, arnaud.videt@univ-lille.fr, nadir.idir@univ-lille.fr
URL: http://l2ep.univ-lille.fr/en/

Acknowledgments

This work has been achieved within the framework of CE2I project (Convertisseur d'Energie Intégré Intelligent). CE2I is co-financed by European Union with the financial support of European Regional Development Fund (ERDF), French state and the French Region of Hauts-de-France.

Keywords

≪Parasitic elements≫, ≪Passive component≫, ≪Electromagnetic Interference (EMI)≫, ≪Passive filters≫, ≪Coupled inductor≫.

Abstract

High-frequency static converters requires inductors, common and differential mode chokes with a low equivalent parallel capacitance. To reduce it, this paper proposes first a semi-analytical model of this capacitance for inductors made with coated ring cores of nano-crystalline material. This model is based on 2D finite element method to compute the turn-turn and turn-core parasitic capacitances, taking into account loose windings. Then the total capacitance is computed thanks to an energetic approach. The model is validated against measurements performed on one core for several numbers of turns. Since the model shows that the capacitance is almost linear with the parasitic turn-core capacitance, specific devices are proposed to increase the distance between turns and core and thus decrease the capacitance. It is demonstrated that a small increase in overall volume allows to divide the equivalent parallel capacitance of a common mode choke by almost a factor of three while increasing its overall volume by only 37%.

Introduction

High frequency power converters ($>$ 100 kHz range) made with GaN and SiC fast switching transistors are prone to high frequency noise that must be reduced to comply with EMC standards [1]. But the inductors used in the low-pass filters are not perfect [2], and their Equivalent Parallel Capacitances (EPC) is a low impedance path for high frequency noise. To gain insights on the way to reduce it, a model is needed. Finite Element Method (FEM) is usually used to simulate the value of the EPC [3, 4, 5, 6] but its relation with geometrical and material parameters is difficult to infer and requires sensitivity analysis. To tackle this black box vision and to increase the speed of computation for optimization purpose [7], several analytical models have been proposed in the literature [8, 9, 10, 11, 12, 13]. Some are specific for transformers with straight core and multilayer windings [8, 9, 11, 12]. Others are dedicated to ring core inductors [10, 13] but fail to reproduce the evolution of the capacitance with an increasing number of turns because of the non-physical potential distribution along the winding. In this paper, a model of the EPC of a ring core inductor with conductive core is proposed. Firstly the potential distribution along the winding and the capacitive network of the winding are described. Secondly this network is solved by an

energetic approach [8, 14, 15]. Then the elementary inter-turns and turn-core capacitances are computed to complete the model. Several analytical formulations are described in [8, 10, 13] but only the ones that take into account tight windings [12, 13] are compared against FEM or measurements in [17]. Since loose windings are of interest in this paper, FEM is preferred. Thirdly the proposed model is compared against measurements. Finally some ways to reduce the EPC are presented in a fourth part thanks to the study of the proposed model.

Description of the common mode choke

The common mode choke is a two windings component that provides a high impedance path to common mode current (thus filtering it) and low impedance path to differential mode current (leakage inductance for a not perfect choke). Figure 1a depicts the component, Fig. 1b and Fig. 1c its equivalent circuit and the common mode equivalent one respectively, with L^* the complex inductance (inductance with losses), EPC the capacitance due to windings, I_{CM} the common mode current, U_L the voltage drop across the choke due to I_{CM}, and V_0 a reference potential. It is assumed that $EPC = 2 \cdot EPC_w$ because of the symmetry of the component and the system which is connected to it.

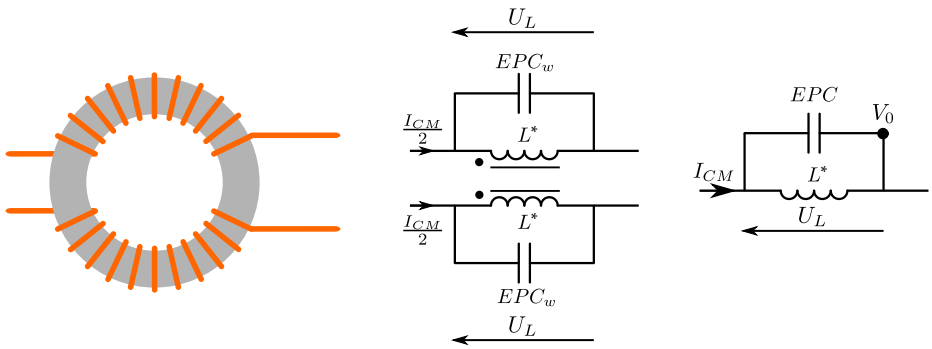

Fig. 1: Common mode inductor and its equivalent circuits: (a) CM inductor top view, (b) two phases equivalent circuit, (c) single-phase equivalent circuit.

Geometry and material

Figure 2a shows a transversal cut of the component. Since the windings are symmetrical, only one half of the choke is drawn, and the N turns of each winding cover an angle β. The core is a ring with a rectangular section as depicted in Fig. 2b with h its height, w its width defined as the difference between the external radius R and the internal radius r. Each face i among the ones described in Fig. 2b ($i \in \{R, r, h\}$, assuming that the top and bottom faces are the same) can be configured by its mid section as in Fig. 2c, with ς_i the maximum turn-core space, s_{tti} the inter-turn space, d_w the copper diameter of the wire, d_{wo} the insulated wire diameter, ε_w its relative permittivity, and e_i the coating thickness of the core with ε_c its relative permittivity.

Capacitive network of one winding

Only one winding is studied because of the symmetry of the component. In Fig. 1b the stray capacitance of one winding is called EPC_w, and the total stray capacitance EPC is equal to two times the EPC_w. The elementary capacitances dC_{tt} and dC_{tc}, presented in Fig. 3a, represent the capacitive couplings between each turns, and between turns and core respectively. These elementary capacitances depends on the position considered on each face of the core. The study of the capacitive network is simplified by considering each turn as a mono-potential closed-loop of perimeter p, as shown in Fig. 3b Then a parasitic capacitance $C_{tt} = \int_p dC_{tt}$ is introduced between each turn, and a parasitic capacitance $C_{tc} = \int_p dC_{tc}$ is placed between each turn and core, as depicted in Fig. 3.

Voltage distribution along one winding

Since all turns are coupled to the same core, they see the same magnetic flux Φ, so according to Lenz law the voltage drop along one turn (between two loops) is $U_{tt} = -d\Phi/dt = U_L/N$, when no propagation

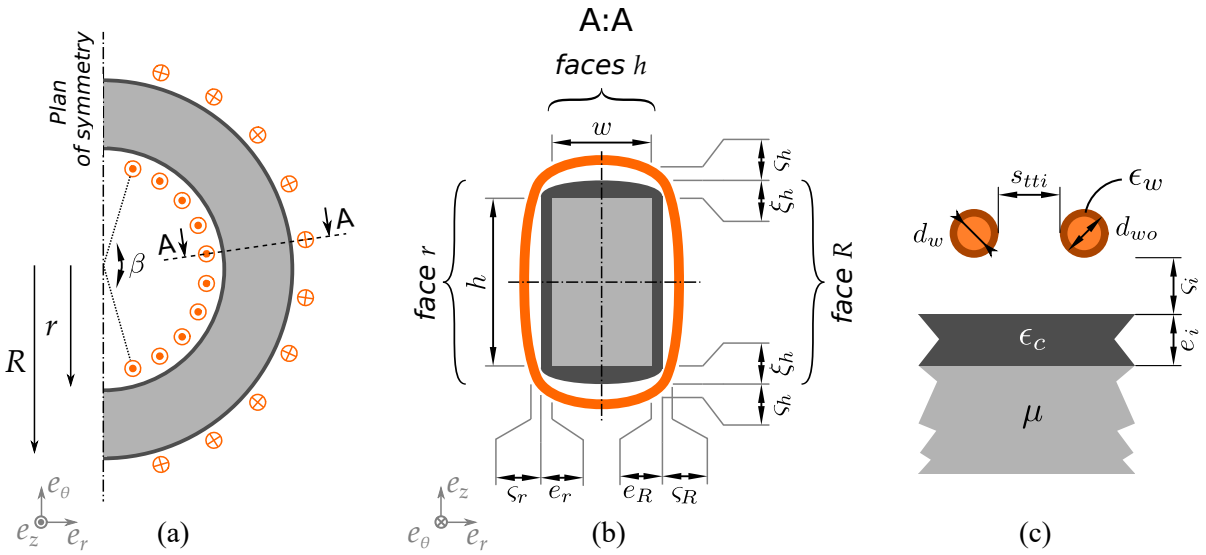

Fig. 2: Description of the geometry of the component: (a) transversal cut, (b) angular cut *A:A* along one turn, (c) close-up of the transverse centre cut of each face *i*.

occurs in the winding. The potential V_n of each loop is chosen as the mid-potential of each turn and is described in (1). The potential of the core $V_c = U_L/2 + V_0$ is the mean potential of the winding because of the symmetry of the capacitive network [9]. An example of potential distribution is shown in Fig. 3c.

$$\forall n \in \mathbb{N}, 1 \leq n \leq N, V_n = \frac{U_{tt}}{2} + (n-1)U_{tt} + V_0 = \frac{2n-1}{2N}U_L + V_0 \tag{1}$$

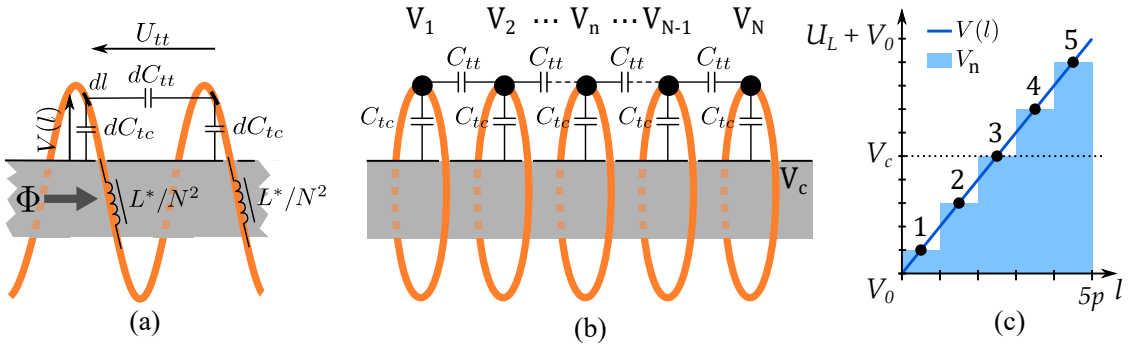

Fig. 3: Capacitive network of one winding: (a) elementary parasitic capacitances, (b) network of parasitic capacitances, (c) an example of the potential distribution along a winding of 5 turns.

Model of the Equivalent Parallel Capacitance

An energetic approach is used to compute the EPC knowing the capacitive network and the voltage across each capacitance in the next subsection. The subsection after shows how the values of inter-turn and turn-core capacitances are determined by FEM.

Computation of the EPC knowing the voltage distribution

The total electrical energy E_{tot} stored in the winding is the sum of the energy of each capacitance as described in (2). Then the EPC as a function of turn number is retrieved as in (3), knowing that the total voltage drop is U_L. For a number of turns N big enough, the EPC is almost a linear function of the turn-core capacitance C_{tc}.

$$E_{tot} = \sum_{1}^{N} \frac{1}{2} C_{tc} \left(\frac{2n - N - 1}{2N} \right)^2 U_L^2 + \sum_{1}^{N-1} \frac{1}{2} C_{tt} \frac{1}{N^2} U_L^2 = \frac{1}{2} \cdot EPC_w \cdot U_L^2 \tag{2}$$

$$EPC_w(N) = \frac{N-1}{N^2} C_{tt} + \frac{1}{12} \frac{N^2 - 1}{N} C_{tc} \tag{3}$$

Determination of C_{tt} and C_{tc} by FEM simulation

The parasitic capacitances C_{tc} and C_{tt} are determined by FEM because loose winding and insulation layers are easily taken into account compared to analytical formulations. To speed up simulations, and simplify the geometry definition in software, 2D FEM is preferred over 3D FEM. Therefore assumptions to make the geometry compatible to 2D are described in the following subsections.

Assumptions for the core coating

The thickness of the coating is assumed to be constant and equal to e_w along the internal and external radii of the core. It is determined from the half difference of the measured coated width of the core w_c and width w as shown in Fig. 4a. The core is assumed to be a perfect conductor to determine the relative permittivity of the coating ε_c . Then the radial capacitance across the cross section of the core is measured and FEM inverse modelling is used to retrieve the value of the permittivity. The radial cut depicted in Fig. 4a shows the setup used to measure the radial capacitance where copper tape is used to make the two surface-probes of potential $V+$ and $V-$ along internal and external radii. Therefore the objective is the minimization of the square of the difference between the measured and simulated capacitances, with ε_c as the design variable. The result is ε_c equal to 2.9 ± 0.5. In addition the Fig. 5b shows that the coating thickness on the top and on the bottom of the core is not constant, its shape is assumed to be parabolic and defined by the function E_h (4), with ξ_h the top of the parabola (deduced from the measurement of the maximum coated height of the core h_c). Therefore the top coating thickness e_h is approximated as the mean of $E_h(x)$, hence the fraction of the maximum thickness (4)

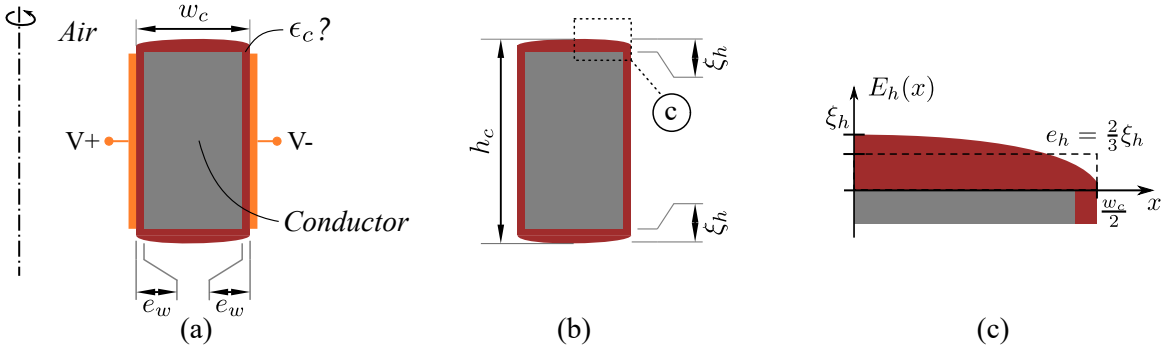

Fig. 4: Characterization of the core coating: (a) cross section of the ring core equipped with copper tape probes $V+$ and $V-$; (b) equivalent circuit of the measured impedance ; (c) close-up of the top coating thickness.

$$\begin{cases} \forall x \in [0, w_c/2], E_h(x) = \xi_h - \xi_h \left(\frac{2x}{w_c} \right)^2 \\ e_h = \frac{2}{w_c} \int_0^{w_c/2} E_h(x) \cdot \mathrm{dx} = 2/3 \cdot \zeta_h \end{cases} \tag{4}$$

Assumptions for the turns

As illustrated in Fig. 5a the wire is not parallel to each face, it is assumed to follow a parabolic curve centered on each face. The coiled height h_b and coiled width w_b of the component are measured at the

top of the parabola made by the turn. To determine C_{tc} and C_{tt} straight geometries are needed, as shown in Fig. 5b. The top and bottom thickness of coating have already been made constant in the previous subsection. The same assumption is used on the turn. The equation of the parabolic curve S_i is presented in (5) with: γ_i the distance between wire conductor and external surface of the core at the end of the face x_i (with $x_i \in \{\frac{w}{2}, \frac{h}{2}\}$) due to either the coating of the wire, or any supplemental material used to insulate or provide space between turn and core ; ς_i the maximum turn-core distance measured at the top of the parabola. Then the turn-core equivalent distance s_{tci} is determined by taking the mean distance under the curve as in (5). Finally the inter-turns spaces along internal and external radii, s_{ttr} and s_{ttR} respectively, are determined from the winding angle β (measured at the middle of wire diameter as depicted in Fig. 2, and for a regular part of winding: for example first and last turn were not taken into account because at the time of measurement they were not aligned with the others) and the measurements of the wounded component external and internal radii R_b and r_b respectively (7). The inter-turn distance on the top and bottom of the core section s_{tth} is assumed to be equal to the mean of the inner and outer inter-turns spaces (7).

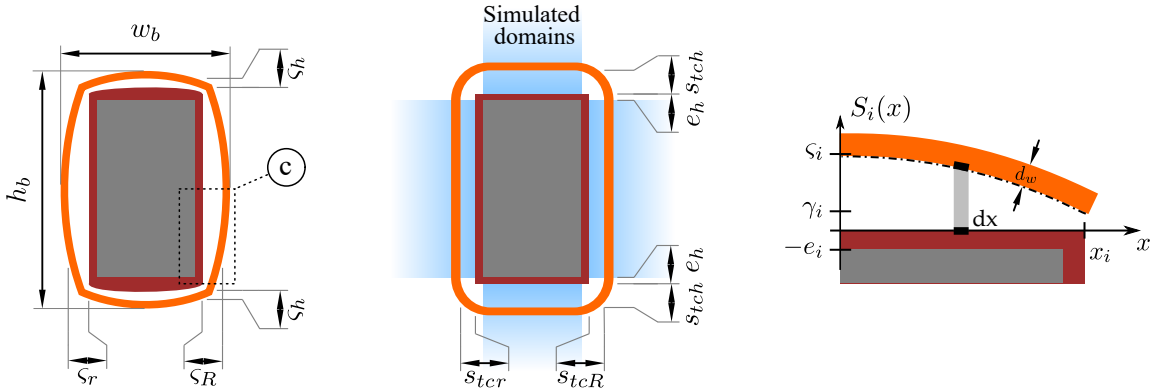

Fig. 5: Simplification of the geometry for 2D simulation: (a) Cross section of the core with one turn, (b) straight geometry resulting from the assumptions performed on the coating, and on the curvature of the turns, (c) close-up on the half-face i and the parabolic turn.

$$\begin{cases} S_i(x) = \varsigma_i - (\varsigma_i - \gamma_i)\left(\frac{x}{x_i}\right)^2 \\ s_{tci} = \frac{1}{x_i}\int_0^{x_i} S_i(x)\cdot \mathrm{dx} = \frac{2}{3}\varsigma_i + \frac{1}{3}\gamma_i \end{cases} \tag{5}$$

$$\begin{cases} \varsigma_r = \varsigma_R & = \frac{1}{2}(w_b - w_c - 2d_{wo}) \\ \varsigma_h & = \frac{1}{2}(h_b - h_c - 2d_{wo}) \end{cases} \tag{6}$$

$$\begin{cases} s_{ttR} & = \frac{1}{N-1}\left(\beta(R_b - \frac{d_{wo}}{2}) - d_{wo}\right) - d_{wo} \\ s_{ttr} & = \frac{1}{N-1}\left(\beta(r_b + \frac{d_{wo}}{2}) - d_{wo}\right) - d_{wo} \\ s_{tth} & = \frac{s_{ttr}+s_{ttR}}{2} \end{cases} \tag{7}$$

Assumptions for the wire insulation

To avoid the meshing of a small thickness, the insulation layer of the wire of thickness $e_w = (d_{wo} - d_w)/2$ is replaced by a portion δ_r of the wire radius r_w, as presented in Fig. 6. Assuming the series capacitances C_w, C_{air} can be approximated with parallel plate capacitances expression (because field lines are almost

radial in the insulation layer), δ_r is chosen to ensure $C_{eq} = C_w \cdot C_{air}/(C_w + C_{air})$ resulting in (8). This leads to a new wire diameter and inter-turn and turn-core spaces $\zeta_{tt,i}$ and ζ_i respectively, as in equation (8). Here ε_w is assumed to be equal to 4 (at 1 MHz, 60°C according to [18]), and e_w is 30 μm according to the data sheet of the wire. Since e_w is closed to the obtained $\delta_r = 22.4$ μm (rel. error +30%), δ_r is chosen to be equal to e_w, and s_{tci}, s_{tti} are leaved unchanged.

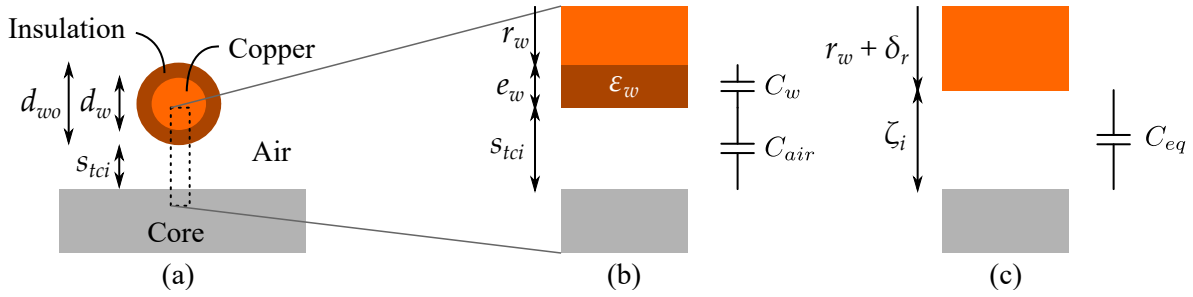

Fig. 6: Compensation of the insulation layer of the wire: (a) transversal cut in the vicinity of a turn, (b) close-up and equivalent capacitance network, (c) close-up of the compensated radius of the wire.

$$\begin{cases} \delta_r & = e_w \left(1 - \frac{1}{\varepsilon_w}\right) \\ \zeta_{tti} & = s_{tti} + e_w - 2\delta_r \\ \zeta_i & = s_{tci} + e_w - \delta_r \end{cases} \tag{8}$$

2D FEM simulation

The parasitic capacitances C_{tci} and C_{tti} between a pair of turns along face i of the core are determined by means of 2D FEM [19]. The section of the geometry is depicted in Fig. 7a and Fig. 7b for C_{tci} and C_{tti} respectively. The depth of the simulation depends on the face i considered (h for simulation along r and R, w for simulation along top and bottom). The total energies E_a and E_b of each simulation in Fig. 7 are used in (9) to retrieve the parasitic capacitance along each face. As expected C_{tti} depends mainly on the inter-turn distance s_{tt} as shown in Fig. 7c and C_{tci} depends not only on turn-core distance s_{tc} but also on inter-turn distance. This is due to E field having more room to reach the core surface from the turn. So s_{tt} is not a degree of freedom to reduce the overall EPC, and should be kept as small as possible. Finally, the total parasitic capacitance C_{tc} and C_{tt} of one turn are computed by adding the contribution of each face (10).

$$\begin{cases} C_{tci} & = \frac{1}{4} E_a \\ C_{tti} & = \frac{1}{2} E_b - \frac{1}{8} E_a \end{cases} \tag{9}$$

$$\begin{cases} C_{tc} & = C_{tcR} + C_{tcr} + 2 \cdot C_{tch} \\ C_{tt} & = C_{ttR} + C_{ttr} + 2 \cdot C_{tth} \end{cases} \tag{10}$$

Experimental validation

An inductor with one winding is used to validate the model of the EPC_w. The core used in this section is a *Vacuumschmelze T60004-L2030 W911*, and named A1 hereafter.

Measurements of the geometry

The nominal uncoated geometry of the core (R, r, h) is known thanks to the data sheet. All the measurements described earlier are performed with a caliper ($\pm$0.02mm). Since the core is not a perfect cylinder,

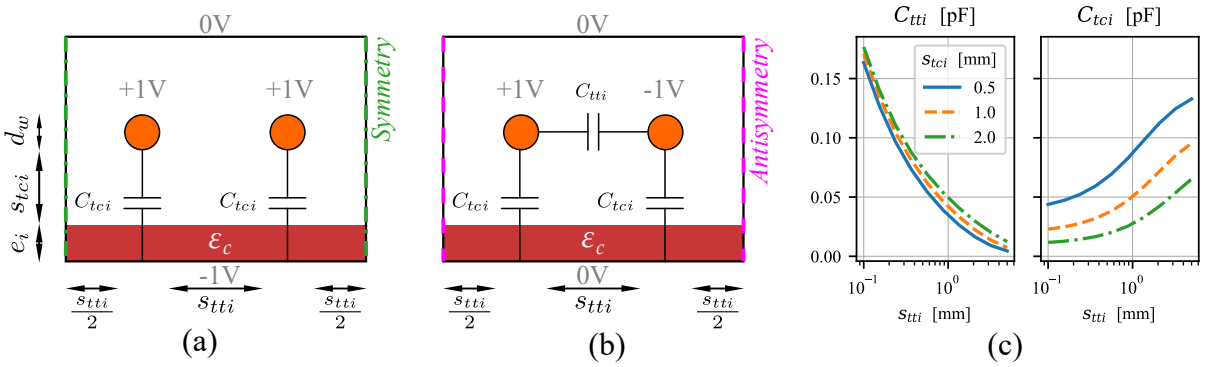

Fig. 7: Simulation of the parasitic capacitances between a pair of turns: (a) determination of C_{tci} with the energy E_a ; (b) determination of C_{tti} knowing C_{tci} and the energy E_b ; (c) evolution of C_{tti}, C_{tci} in function of s_{tti}, s_{tci} with $d_w = 0.56$ mm.

several measurements are performed and the mean of the maximum and minimum values is kept as the nominal one. The uncertainties are equal to the half difference between the maximum and minimum values. All measured values are summarized in Table I (A1 is the current geometry, A2 and A3 are presented in the following section).

	A1 x_{nom}	A1 Δx	A2 x_{nom}	A2 Δx	A3 x_{nom}	A3 Δx
R_c	15.14	0.04	15.14	0.07	15.11	0.05
h_c	11.62	0.04	11.58	0.02	11.67	0.03
w_c	5.39	0.07	5.39	0.05	5.36	0.04
R_b	16.20	0.11	17.03	0.12	17.67	0.14
r_b	8.95	0.05	7.38	0.13	7.18	0.04
h_b	12.85	0.07	14.70	0.25	16.46	0.08
w_b	8.06	0.25	9.98	0.19	10.42	0.23
β [°]	110 for N=28		144 for N=29		136 for N=29	

Table I: Measured variables of the components of A series, in [mm] unless specified otherwise

Measurement of the EPC

The EPC of the component (with either one or two windings) is extracted from the impedance measurement performed with the impedance analyzer *HP4294A* (equipped with the *16047E* socket, and with core standing on its leads at 2 cm over the socket). Fitting is used to find the EPC knowing the measured impedance and the perfect impedance built with the measured inductance factor A_L and the number of turns N. This procedure is repeated for N varying from 30 to 50, by step of 5.

Comparison of the models against the measurements

The measurements described in the previous subsection are compared to the model. To compute the EPC_w the capacitances C_{tc}, C_{tt} are simulated for each face as described previously, then the values are injected in (3) with the number of turns N. In addition to the nominal value, two extrema of EPC_w are calculated: the minimum one given by the maximal value of the distance between turns and the uncoated core $s_{tci} + e_i$, and minimal value of ε_c; the maximum one is the opposite. Fig. 8a illustrates the evolution of EPC_w with the number of turns N. The model is able to reproduce the increase with N, but the nominal relative error of the model to the measurements is between -32% and -27%. Even with the measurement errors on $s_{tc,i}, e_i$ and ε_c taken into account the relative error is reduced but still between -6% and -12%. The origin of this discrepancy might be the hypotheses used to make the geometry straight in the previous section. The deviation at 35 turns in the measured EPC shows also the influence of a not regular turns distribution. The Fig. 8b shows the impedances over the frequency of A1 in comparison to the modelled impedance with the nominal value of EPC_w.The capacitive effect is satisfactorily modelled up to more than 10MHz. As expected however, at frequency greater than 20MHz

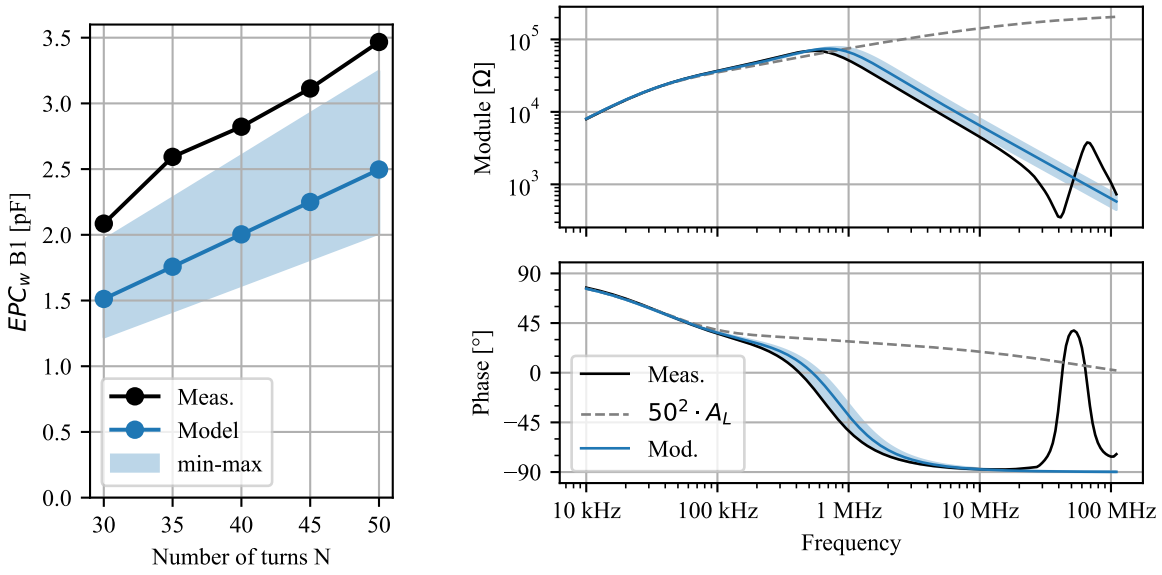

(a) EPC_w of A1

(b) Impedance of A1 at $N = 50$ turns, compared with the nominal value for the model

Fig. 8: Comparison of the measurements and the model of EPC_w

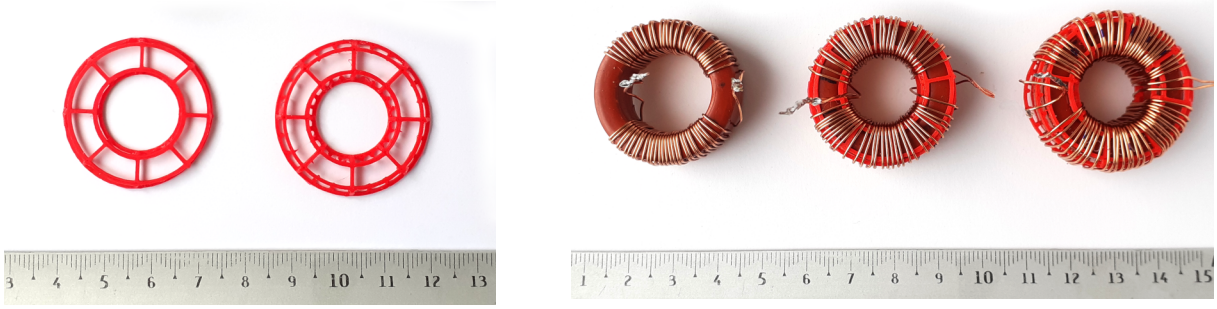

(a) Spacers made with PLA

(b) Common mode chokes equipped with the contraption (from left to right A1, A2 and A3)

Fig. 9: Common mode chokes with different turn-core distance s_{tc}

the simple L*C parallel model is not capable of reproducing the resonances due to propagation along the winding.

Minimization of the parasitic capacitance

According to (3) the effort to reduce EPC for a given number of turns N should be performed on the reduction of the value of C_{tc}. As seen before s_{tti} should be kept as small as possible. Then C_{tc} is qualitatively proportional to the perimeter of each turn p and inversely proportional to the distance s_{tc} between turn and core. An action based on the latter is proposed in the following subsection, and measurements are shown in the following one.

Design of a device to move the turns away from the core

A specific device has been designed in this paper to provide different distances between turn and core. This device has been 3D printed with Poly-Lactic-Acid (PLA) thermoplastic and is presented in Fig. 9a. Three ring cores of the previously used reference have been wound with two windings of 30 turns in common mode, as seen in Fig. 9b. The first one is a control one and named $A1$ while $A2$ and $A3$ are equipped with a device with a theoretical thickness of respectively 0.8 mm and 1.6 mm.

Measurements of the EPC for different turn-core distances

The *EPC* of the *A* series have been extracted as specified before, and compared to the model computed as in the previous section in Fig. 9a (with the relative permittivity of PLA neglected). In comparison to A1, the *EPC* is divided by a factor of 2.9 and 3.7 for A2 and A3 respectively, which is translated by a shift of the resonant frequency of respectively 1.7 and 1.9 to the right as seen in Fig. 10b. Meanwhile the dead volume (volume of the cylinder taken by the core and its windings) of each component has been increased by 37% and 54% for A2 and A3 respectively. As expected the *EPC* is almost inversely proportional to the distance between turns and core. So a small increase in s_{tc} decreases significantly the *EPC* with a reasonable penalty on the volume, which makes it an interesting way to improve the high-frequency behaviour of CM chokes. The model gives the correct order of magnitude and evolution of EPC with turn-core distance, but the relative error for the nominal case is between -36% and -28%. In addition the min-max range is reduced around the nominal case for A2 and A3 in comparison to A1. It seems likely that the hypotheses used in the model underestimates the value of the EPC for and that their impact is smaller for loose winding.

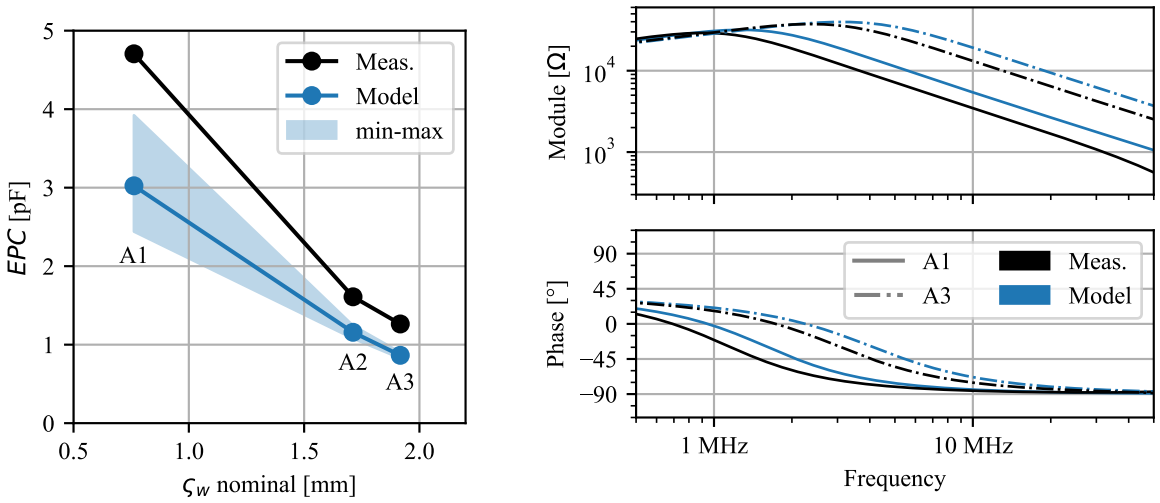

(a) *EPC* of the cores from the B serie

(b) Impedance of the cores from the A serie, compared with the model at nominal value

Fig. 10: Comparison of the measurements and the model of *EPC* with different turn-core distances

Conclusion

The proposed model gives a satisfactory estimation of the EPC of inductors made with ring core of nano-crystalline material. The use of 2D FEM allows quick computation of the inter-turn and turn-core parasitic capacitances and the modelling of loose windings and coatings. The increase of the EPC with the number of turns for a given core is correctly predicted by the model. According to this model the main part of the EPC is due to the turn-core parasitic capacitance. This is why a device has been realized to move away the turns from the core and thus to decrease the EPC. The results shows that a small increase of the turn-core distance is enough to significantly reduce the EPC. The perspectives of this work are first proper uncertainties propagation to help in the refinement of the modelling hypotheses and to increase the accuracy of the model, second the optimization of the spacers with application constraints, and finally the extension of the model to the more frequently used ferrite materials. The use of this model for the sizing of common mode chokes would improve their high frequency effectiveness for filtering applications.

References

[1] A. K. Morya et al., "Wide Bandgap Devices in AC Electric Drives: Opportunities and Challenges," in IEEE Transactions on Transportation Electrification, vol. 5, no. 1, pp. 3-20, March 2019, doi: 10.1109/TTE.2019.2892807.

[2] Shuo Wang, F. C. Lee, D. Y. Chen and W. G. Odendaal, "Effects of parasitic parameters on EMI filter performance," in IEEE Transactions on Power Electronics, vol. 19, no. 3, pp. 869-877, May 2004, doi: 10.1109/TPEL.2004.826527.

[3] M. Kovačić, S. Stipetić, Z. Hanić and D. Žarko, "Small-Signal Calculation of Common-Mode Choke Characteristics Using Finite-Element Method," in IEEE Transactions on Electromagnetic Compatibility, vol. 57, no. 1, pp. 93-101, Feb. 2015, doi: 10.1109/TEMC.2014.2362998.

[4] A. Chafi, N. Idir, A. Videt and H. Maher, "Design Method of PCB Inductors for High-Frequency GaN Converters," in IEEE Transactions on Power Electronics, vol. 36, no. 1, pp. 805-814, Jan. 2021, doi: 10.1109/TPEL.2020.3000438.

[5] C. Cuellar et N. Idir, « Stray capacitances determination methods of EMI filter inductors », in IECON 2017 - 43rd Annual Conference of the IEEE Industrial Electronics Society, oct. 2017, p. 7040-7045. doi: 10.1109/IECON.2017.8217231.

[6] M. Bensetti et al., "A hybrid finite-element method for the modeling of microcoils," in IEEE Transactions on Magnetics, vol. 41, no. 5, pp. 1868-1871, May 2005, doi: 10.1109/TMAG.2005.846284.

[7] B. Zaidi, A. Videt and N. Idir, "Optimization Method of CM Inductor Volume Taking Into Account the Magnetic Core Saturation Issues," in IEEE Transactions on Power Electronics, vol. 34, no. 5, pp. 4279-4291, May 2019, doi: 10.1109/TPEL.2018.2861620.

[8] H. Zhao et al., "Physics-Based Modeling of Parasitic Capacitance in Medium-Voltage Filter Inductors," in IEEE Transactions on Power Electronics, vol. 36, no. 1, pp. 829-843, Jan. 2021, doi: 10.1109/TPEL.2020.3003157.

[9] Z. Shen, H. Wang, Y. Shen, Z. Qin and F. Blaabjerg, "An Improved Stray Capacitance Model for Inductors," in IEEE Transactions on Power Electronics, vol. 34, no. 11, pp. 11153-11170, Nov. 2019, doi: 10.1109/TPEL.2019.2897787.

[10] G. Dong, F. Zhang, Y. Liu, W. Meng and C. Xu, "Analytical Method for Extraction of Stray Capacitance in Single-Layer CM Chokes," 2019 IEEE Energy Conversion Congress and Exposition (ECCE), 2019, pp. 3185-3191, doi: 10.1109/ECCE.2019.8912846.

[11] W. Tan, X. Margueron and N. Idir, "Analytical modeling of parasitic capacitances for a planar common mode inductor in EMI filters," 2012 15th International Power Electronics and Motion Control Conference (EPE/PEMC), 2012, pp. DS3f.2-1-DS3f.2-6, doi: 10.1109/EPEPEMC.2012.6397368.

[12] L. Dalessandro, F. da Silveira Cavalcante and J. W. Kolar, "Self-Capacitance of High-Voltage Transformers," in IEEE Transactions on Power Electronics, vol. 22, no. 5, pp. 2081-2092, Sept. 2007, doi: 10.1109/TPEL.2007.904252.

[13] A. Massarini and M. K. Kazimierczuk, "Self-capacitance of inductors," in IEEE Transactions on Power Electronics, vol. 12, no. 4, pp. 671-676, July 1997, doi: 10.1109/63.602562.

[14] J. Biela and J. W. Kolar, "Using Transformer Parasitics for Resonant Converters—A Review of the Calculation of the Stray Capacitance of Transformers," in IEEE Transactions on Industry Applications, vol. 44, no. 1, pp. 223-233, Jan.-feb. 2008, doi: 10.1109/TIA.2007.912722.

[15] E. C. Snelling, Soft Ferrites : Properties and applications. London: Iliffe Books Ltd, 1969.

[16] Y. Li and S. Wang, "Modeling and Increasing the High-Frequency Impedance of Single-Layer Mn-Zn Ferrite Toroidal Inductors With Electromagnetic Analysis," in IEEE Transactions on Power Electronics, vol. 36, no. 6, pp. 6943-6953, June 2021, doi: 10.1109/TPEL.2020.3039809.

[17] N. B. Chagas and T. B. Marchesan, "Analytical Calculation of Static Capacitance for High-Frequency Inductors and Transformers," in IEEE Transactions on Power Electronics, vol. 34, no. 2, pp. 1672-1682, Feb. 2019, doi: 10.1109/TPEL.2018.2829716.

[18] S. Diaham and M.-L. Locatelli, 'Dielectric properties of polyamide-imide', J. Phys. D: Appl. Phys., vol. 46, no. 18, p. 185302, Apr. 2013, doi: 10.1088/0022-3727/46/18/185302.

[19] C. Meeker, FEMM 4.2 (build Apr. 21, 2019) [Online]. Available: https://www.femm.info